Available online at www.sciencedirect.com
ScienceDirect
Comput. Methods Appl. Mech. Engrg. 196 (2007) 2972–2980
Computer methods in applied mechanics and engineering
www.elsevier.com/locate/cma

A computational framework for network modeling of fibrous biological tissue deformation and rupture

T.I. Zohdi *

Department of Mechanical Engineering, 6195 Etcheverry Hall, University of California, Berkeley, CA 94720-1740, USA

Received 12 November 2005; received in revised form 5 March 2006; accepted 9 June 2006

Abstract

The tremendous increase in accessible, powerful, desktop computers has raised the possibility of rapid high speed simulation of the response of fibrous biological tissue using networks of fibers to represent the load bearing component of such materials. The purpose of this paper is to present a relatively simple, robust, *modeling and computational framework*, based on fiber networks, which can be implemented with minimal effort by researchers in the biomechanics community, and which is relatively easy to tailor to specific applications. The advantages of such a fiber network approach are (1) the simplicity of the constitutive laws at the fiber level, for example relaxed one-dimensional Fung material laws, (2) the ability to easily incorporate effects such as fiber damage and rupture and (3) the amenability of the model to extremely rapid numerical simulation.
© 2007 Elsevier B.V. All rights reserved.

Keywords: Biological tissue; Rupture; Networks; Computations

1. Introduction

Fibrous material represents the load bearing component of many types of soft biological tissue. For overviews of a wide variety of soft tissue continuum models, see the extensive works of Holzapfel and coworkers [20–24] and Humphrey and coworkers [25–35]. Models which explicitly account for the presence of fibers in biological tissue date back, at least, to Lanir [36], who formulated continuum models based on the existence of fiber families. For a review of Lanir-type models, as well as other classes of biological constitutive models, see the review of Sacks and Sun [47].[1] Below the (homogenized) continuum scale, such material exhibits a microstructure comprised of fibers embedded within a soft tissue matrix. At the homogenized continuum scale, this frequently results in macroscopically anisotropic material behavior, which is difficult to properly mathematically formulate at finite strains, in particular if anisotropic damage and rupture effects are to be taken into account. The specific type of *global* anisotropy is irrelevant to the solution technique to be presented, since it starts at a scale where the fibers are treated as a network of interconnected links. *The purpose of this work is to present a relatively simple, robust, modeling and computational framework, based on fiber networks*, which usually comprise the load bearing component of many types of biological tissue, which can be implemented with minimal effort by researchers in the field, and which is relatively easy to tailor to specific applications. The advantages of such a fiber network approach are that the constitutive laws at the fiber level can be represented simple one-dimensional constitutive laws and that damage and rupture of these fibers is easy to characterize and rapidly computable.

We consider a model problem structure comprised of an initially undeformed surface network of one-dimensional fibers (Fig. 1). The structure is capable deforming in three dimensions (in and out of the initial plane), in response to

* Tel.: +1 510 642 6834; fax: +1 510 642 6163.
E-mail address: zohdi@me.berkeley.edu
[1] Also see the paper of Costa et al. [9], among numerous others.

0045-7825/$ - see front matter © 2007 Elsevier B.V. All rights reserved.
doi:10.1016/j.cma.2006.06.015

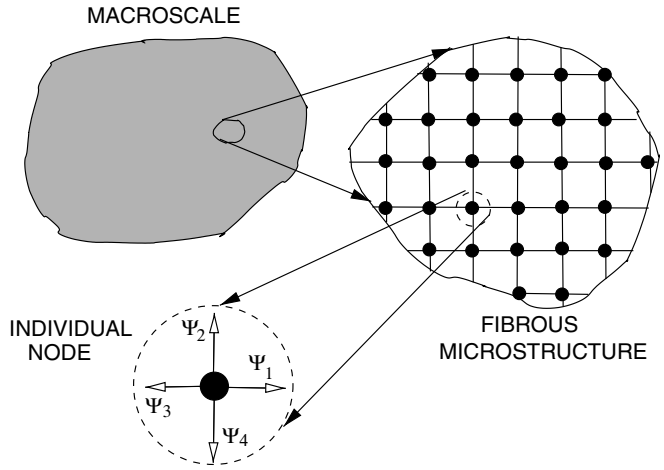

Fig. 1. An idealized fiber network with heterogeneous fibers.

loading on its surface. The fibers are joined at the nodes (as pinned-joints), in other words, they are sutured together at those locations to form a network. While the structure is relatively simple, compared with real biological tissue, the primary purpose here is to illustrate how the approach works, since it is quite flexible, and adaptable to specific applications. In the present analysis, the soft web-tissue contribution to the response is considered negligible relative to that of the relatively stiff load carrying fibers. By employing enough of these simple structural elements, one can build an entire macroscale sheet of fibrous tissue, as shown in Fig. 1.

We shall consider scenarios where we may assume that, for load bearing soft tissue, the compressive response is of minor interest. A type of modeling approach that is ideal to describe such situations is the relaxed theory of perfectly flexible solids, which entails enforcing a zero stress state for any compressive strains. Early mathematical analysis of such models can be credited to Pipkin [44] who considered a minimizing sequence for an associated variational problem, and showed that such sequences exhibit structure similar to that observed in wrinkling of thin elastic sheets. Several researchers have adopted similar approaches for the elastostatic analysis of structural fabric; for example Buchholdt et al. [4], Pangiotopoulos [42], Bufler and Nguyen-Tuong [5] and Cannarozzi [6,7]. Notable is the work of Steigmann and coworkers [50,17–19,1,2], who developed a series of theoretical results and elastostatic solution techniques based on pseudo-dynamic relaxation methods, similar to those found in Papadrakakis [43]. In particular, Steigmann and coworkers have shown that a necessary condition for the existence of energy minimizers in elastostatics is for the structural members to carry no load in compression. This model has served as a foundation for more elaborate models describing rupture of ballistic fabric shielding in Zohdi and Steigmann [61], Zohdi [62] and Zohdi and Powell [63], of which the present approach builds upon.

2. Modeling individual biological fibers

The starting point for the analysis is a *purely one-dimensional* microscale description of the tensile deformation of a fiber, employing the mentioned relaxed methodology for each fiber. Although the upcoming analysis is general, for brevity, we employ a classical one-dimensional Fung material model for the fibers [13–15].[2] The stored energy of a single Fung fiber is given by

$$W = c(\mathrm{e}^{Q} - 1), \tag{2.1}$$

where $Q = \frac{1}{2}HE^2$, H and c are material constants, $E \overset{\text{def}}{=} \frac{1}{2}(C-1)$ is the Green–Lagrange strain, $C \overset{\text{def}}{=} F^2$ is the right Cauchy–Green strain, $F = \frac{\mathrm{d}x}{\mathrm{d}X}$ is the deformation gradient, X are referential coordinates and x are current coordinates along the axis of the fiber. The exponential term phenomenologically describes a stiffening effect, due to a progressive reduction in fibrous microscale "slack", which is prevalent in many types biological tissue. The second Piola–Kirchhoff stress is given by

$$S = \frac{\partial W}{\partial E} = c\frac{\partial Q}{\partial E}\mathrm{e}^{Q} = cHE\mathrm{e}^{\frac{HE^2}{2}}, \tag{2.2}$$

and the tangent stiffness is

$$\frac{\partial^2 W}{\partial E^2} = c\mathrm{e}^{Q}\left(\frac{\partial Q}{\partial E}\right)^2 + c\mathrm{e}^{Q}\frac{\partial^2 Q}{\partial E^2} = cH\mathrm{e}^{Q}(1+HE^2). \tag{2.3}$$

We remark that, during the calculations, it is convenient to work with quantities expressed in terms of the stretch ratio, $U = \frac{L}{L_{\mathrm{o}}}$, where L is the deformed length of the fiber, L_{o} is its original length and, by virtue of a polar-decomposition, $E = \frac{1}{2}(U^2-1)$. *For this relaxed one-dimensional model*, since the Cauchy stress, σ, is related to the second Piola–Kirchhoff stress by $\sigma = \frac{1}{J}F^2S$, where J is the Jacobian of F, we need only be concerned with $F \geqslant 1$, thus, $J = F$, and consequently, $\sigma = FS$.

Remark 1. This relaxed (tensile-strain only) one-dimensional model is trivially polyconvex, which is a desirable (sufficient) property from a mathematical existence theory standpoint. Recall, a general three-dimensional stored energy function is polyconvex if, for two deformation gradients, $\boldsymbol{F}$ and $\boldsymbol{G}$

$$\begin{aligned} &W(\theta(\boldsymbol{F}, \operatorname{cof}\boldsymbol{F}, \det\boldsymbol{F}) + (1-\theta)(\boldsymbol{G}, \operatorname{cof}\boldsymbol{G}, \det\boldsymbol{G})) \\ &\quad \leqslant \theta W(\boldsymbol{F}, \operatorname{cof}\boldsymbol{F}, \det\boldsymbol{F}) + (1-\theta)W(\boldsymbol{G}, \operatorname{cof}\boldsymbol{G}, \det\boldsymbol{G}), \end{aligned} \tag{2.4}$$

where $\operatorname{cof}\boldsymbol{F} = \boldsymbol{F}^{-\mathrm{T}}\det\boldsymbol{F}$ and $0 \leqslant \theta \leqslant 1$. In one dimension, for tensile states only, the tensorial quantities take on the form $\boldsymbol{F} = F$, $\operatorname{cof}\boldsymbol{F} = 1$ and $\det\boldsymbol{F} = F$. Thus, for the one-dimensional relaxed theory, convexity of $W(F)$ in F is equivalent to polyconvexity. By computing two derivatives of $W(F)$, and enforcing $\frac{\partial^2 W}{\partial F^2} > 0$ for convexity, we obtain

[2] The well-known difficulties and ambiguities with the three-dimensional Fung model are irrelevant for this one-dimensional analysis.

$$\frac{\partial^2 W}{\partial F^2} = c e^{Q}\left(\frac{\partial Q}{\partial F}\right)^2 + c e^{Q}\frac{\partial^2 Q}{\partial F^2} > 0, \tag{2.5}$$

which is valid for positive values of c and H or if both constants are negative. The canonical choice is that they are both positive, which we adopt. We note that the tangent stiffness can be represented as

$$\frac{\partial^2 W}{\partial E^2} = \frac{\partial^2 W}{\partial F^2}F^{-2} - \frac{\partial W}{\partial F}F^{-3}, \tag{2.6}$$

thus illustrating that polyconvexity and positive-definiteness of the tangent stiffness are clearly different conditions.

Remark 2. While it is generally not true that the compressive response of fibrous tissues is always of little interest, in this paper we formulate only a compression-free model, primarily because we are interested in tensile tearing type failure of soft tissue. However, it is important to note that, for example, cartilage researchers believe that the difference between the tensile and compressive properties of that fibrous tissue are the key to understanding its response to dynamic loading. For example, one of the more important problems in tendon mechanics is understanding the tendon-to-bone insertion (especially its repair), which most surgeons believe places the tendon under compression. The natural loading state of pressurized structures such as arteries and the heart places the tissue in radial compression, and this is sometimes important to the mechanics (especially as it relates to wall thickening in the heart). Thus, there are clearly many biomechanics applications where compression can play a role, and the method developed can be extended to those regimes with relatively minor modifications.

3. Fiber rupture

The simplest approach to describe failure of a fiber is to check whether a critical stretch has been attained, $U(t) \geqslant U_{\text{crit}}$. If this condition is met, then the fiber is deemed inactive. However, it is more realistic to have the fiber gradually rupture. In order to track the progressive damage for the Ith fiber, a single damage variable, α_I, is used. The damage variable α_I can, for example, represent the fraction of smaller scale fibrils that are *not ruptured*, within the Ith fiber.[3] Thus, for a fiber that is undamaged, $\alpha_I = 1$, while for an fiber that is completely damaged, $\alpha_I = 0$. Probably the simplest damage representation is, with $\alpha_I(t=0) = 1$

$$\alpha_I(t) = \min\left(\alpha_I(0 \leqslant t^* < t), e^{\left(-\lambda\left(\frac{U(t)-U_{\text{crit}}}{U_{\text{crit}}}\right)\right)}\right), \tag{3.1}$$

where $U(t)$ is the stretch of the fiber at time t, and where $0 \leqslant \lambda$ is a rate parameter. The above relation indicates that damage is irreversible, i.e. α_I is a monotonically decreasing function. As $\lambda \to \infty$, the type of failure tends towards sudden rupture, while as $\lambda \to 0$, then there is no damage generated.

4. Simulation of tissue dynamics

A natural way to simulate the dynamics of such tissue is to consider a lumped mass model, where the lumped masses are located at the suture (criss-cross) points (Fig. 1).

4.1. Lumped mass representation

The connection points are pinned-joints. For each lumped mass, dynamic equilibrium is computed via

$$m\ddot{\boldsymbol{r}}_i = \underbrace{\boldsymbol{\psi}_i^{\text{tot}}}_{\text{total}} = \underbrace{\boldsymbol{\psi}_i^{\text{ext}}}_{\text{applied forces}} + \underbrace{\sum_{I=1}^{4}\boldsymbol{\psi}_{iI}}_{\text{surrounding fibers}} \tag{4.1}$$

for $i = 1, 2, \ldots, N$, where N is the number of lumped masses (nodes), where the summed four forces ($\boldsymbol{\psi}_{iI}$) are the axial contributions of the four fiber intersecting at node i (Fig. 1), where $\boldsymbol{\psi}_i^{\text{ext}}$ is the applied external force contribution and where m is the mass of a single lumped mass node, i.e. the total tissue mass divided by the total number of nodes. To determine the forces from the fibers acting on a lumped mass, one simply computes the product of the Cauchy stress and the cross-sectional area. Accordingly, the contribution of the Ith fiber to the ith lumped mass is $\boldsymbol{\psi}_{iI} = S_I U_I A_0 \boldsymbol{a}_{iI}$ (A_0 is the cross-sectional area of fiber), where the unit axial fiber direction is given by $\boldsymbol{a}_{iI} = \frac{\boldsymbol{r}_I^+ - \boldsymbol{r}_I^-}{\|\boldsymbol{r}_I^+ - \boldsymbol{r}_I^-\|}$, where $\boldsymbol{r}_I^+$ denotes the endpoint not in contact with the lumped mass and $\boldsymbol{r}_I^-$ denotes the endpoint in contact with the lumped mass (Fig. 1).[4] Clearly, $\boldsymbol{\psi}_{iI}$ is a function of $\boldsymbol{r}_i$. In order to determine the deformation and damaged state of the fibers, the nodal positions of the network must be determined. In order to handle a system such as that described in Eq. (4.1), which is coupled to Eq. (3.1), we develop an iterative fixed-point scheme next.

4.2. Temporal discretization and adaptivity

Implicit time-stepping methods, with time step size adaptivity, built on approaches found in Zohdi [54–58], will be used throughout the upcoming analysis. Accordingly, after time discretization of the acceleration term in the equations of motion (Eq. (4.1)) for a lumped mass:

$$\ddot{\boldsymbol{r}}_i^{L+1} \approx \frac{\boldsymbol{r}_i^{L+1} - 2\boldsymbol{r}_i^{L} + \boldsymbol{r}_i^{L-1}}{(\Delta t)^2}, \tag{4.2}$$

where, for brevity, we denote $\boldsymbol{r}_i^{L+1} \stackrel{\text{def}}{=} \boldsymbol{r}_i(t+\Delta t)$ (L is a time step counter), $\boldsymbol{r}_i^{L} \stackrel{\text{def}}{=} \boldsymbol{r}_i(t)$, etc., one can arrive at the following abstract form, for the entire system:

$$\mathscr{A}(\boldsymbol{r}^{L+1}) = \mathscr{F}. \tag{4.3}$$

[3] This topic, which is relevant in a multiscale setting, has been explored in depth in Zohdi and Steigmann [61] and Zohdi and Powell [63].

[4] $\|\cdot\|$ indicates the Euclidean norm in R^3.

It is convenient to write

$$\mathscr{A}(\boldsymbol{r}^{L+1}) - \mathscr{F} = \mathscr{G}(\boldsymbol{r}^{L+1}) - \boldsymbol{r}^{L+1} + \mathscr{E} = 0, \tag{4.4}$$

where $\mathscr{E}$ is a remainder term which does not depend on the solution, i.e. $\mathscr{E} \neq \mathscr{E}(\boldsymbol{r}^{L+1})$. A straightforward iterative scheme can be written as

$$\boldsymbol{r}^{L+1,K} = \mathscr{G}(\boldsymbol{r}^{L+1,K-1}) + \mathscr{E}, \tag{4.5}$$

where $K = 1, 2, 3, \ldots$ is the index of iteration within time step $L+1$. The convergence of such a scheme is dependent on the behavior of $\mathscr{G}$. Namely, a sufficient condition for convergence is that $\mathscr{G}$ is a contraction mapping for all $\boldsymbol{r}^{L+1,K}$, $K = 1, 2, 3 \ldots$ In order to investigate this further, we define the error as

$$\boldsymbol{\varpi}^{L+1,K} = \boldsymbol{r}^{L+1,K} - \boldsymbol{r}^{L+1}. \tag{4.6}$$

A necessary restriction for convergence is iterative self consistency, i.e. the exact solution must be represented by the scheme

$$\mathscr{G}(\boldsymbol{r}^{L+1}) + \mathscr{E} = \boldsymbol{r}^{L+1}. \tag{4.7}$$

Enforcing this restriction, a sufficient condition for convergence is the existence of a contraction mapping

$$\begin{aligned} \|\boldsymbol{\varpi}^{L+1,K}\| &= \|\boldsymbol{r}^{L+1,K} - \boldsymbol{r}^{L+1}\| \\ &= \|\mathscr{G}(\boldsymbol{r}^{L+1,K-1}) - \mathscr{G}(\boldsymbol{r}^{L+1})\| \\ &\leqslant \eta^{L+1,K}\|\boldsymbol{r}^{L+1,K-1} - \boldsymbol{r}^{L+1}\|, \end{aligned} \tag{4.8}$$

where, if $\eta^{L+1,K} < 1$ for each iteration K, then $\varpi^{L+1,K} \to 0$ for any arbitrary starting value $\boldsymbol{r}^{L+1,K=0}$ as $K \to \infty$. The type of contraction condition discussed is sufficient, but not necessary, for convergence. In order to control convergence, we modify the discretization of the acceleration term[5]:

$$\ddot{\boldsymbol{r}}^{L+1} \approx \frac{\dot{\boldsymbol{r}}^{L+1} - \dot{\boldsymbol{r}}^{L}}{\Delta t} \approx \frac{\frac{\boldsymbol{r}^{L+1} - \boldsymbol{r}^{L}}{\Delta t} - \dot{\boldsymbol{r}}^{L}}{\Delta t} \approx \frac{\boldsymbol{r}^{L+1} - \boldsymbol{r}^{L}}{\Delta t^2} - \frac{\dot{\boldsymbol{r}}^{L}}{\Delta t}. \tag{4.9}$$

Inserting this into $m\ddot{\boldsymbol{r}} = \boldsymbol{\Psi}^{\mathrm{tot}}(\boldsymbol{r})$ leads to

$$\boldsymbol{r}^{L+1,K} \approx \underbrace{\frac{\Delta t^2}{m}(\boldsymbol{\Psi}^{\mathrm{tot}}(\boldsymbol{r}^{L+1,K-1}))}_{\mathscr{G}(\boldsymbol{r}^{L+1,K-1})} + \underbrace{(\boldsymbol{r}^{L} + \Delta t \dot{\boldsymbol{r}}^{L})}_{\mathscr{E}}, \tag{4.10}$$

whose convergence is restricted by $\eta \propto EIG(\mathscr{G}) \propto \frac{\Delta t^2}{m}$. Therefore, we see that the eigenvalues of $\mathscr{G}$ are (1) directly dependent on the strength of the interaction forces, (2) inversely proportional to the mass and (3) directly proportional to $(\Delta t)^2$. Therefore, if convergence is slow within a time step, the time step size, which is adjustable, can be reduced by an appropriate amount to increase the rate of convergence. Thus, decreasing the time step size improves the convergence, however, we want to simultaneously maximize the time step sizes to decrease overall computing time, while still meeting an error tolerance. In order to achieve this goal, we follow an approach found in Zohdi [54–58] originally developed for continuum thermo-chemical multifield problems in which (1) one approximates $\eta^{L+1,K} \approx \gamma(\Delta t)^p$ (γ is a constant) and (2) one approximates the error within an iteration to behave according to

$$(\gamma(\Delta t)^p)^K \|\boldsymbol{\varpi}^{L+1,0}\| = \|\boldsymbol{\varpi}^{L+1,K}\|, \quad K = 1, 2, \ldots, \tag{4.11}$$

where $\|\boldsymbol{\varpi}^{L+1,0}\|$ is the initial norm of the iterative error and γ is a function intrinsic to the system.[6] Our goal is to meet an error tolerance in exactly a preset number of iterations. In the definition of the error, since the "true" solution at a time step, $\boldsymbol{r}^{L+1}$, is unknown, we use the most current value of the solution, $\boldsymbol{r}^{L,K}$, thus the error is to be interpreted as the relative error. To this end, one writes this in the following approximate form:

$$(\gamma(\Delta t_{\mathrm{tol}})^p)^{K_{\mathrm{d}}} \|\boldsymbol{\varpi}^{L+1,0}\| = \mathrm{TOL}, \tag{4.12}$$

where TOL is a tolerance and where K_{d} is the number of desired iterations.[7] If the error tolerance is not met in the desired number of iterations, the contraction constant $\eta^{L+1,K}$ is too large. Accordingly, one can solve for a new smaller step size, under the assumption that γ is constant:

$$\Delta t_{\mathrm{tol}} = \Delta t \left(\frac{\left(\frac{\mathrm{TOL}}{\|\boldsymbol{\varpi}^{L+1,0}\|}\right)^{\frac{1}{pK_{\mathrm{d}}}}}{\left(\frac{\|\boldsymbol{\varpi}^{L+1,K}\|}{\|\boldsymbol{\varpi}^{L+1,0}\|}\right)^{\frac{1}{pK}}} \right). \tag{4.13}$$

The assumption that γ is constant is not critical, since the time steps are to be recursively refined and unrefined repeatedly. Clearly, the expression in Eq. (4.13) can also be used for time step enlargement, if convergence is met in less than K_{d} iterations. Classical solution methods require $\mathscr{O}(N^3)$ operations, whereas iterative schemes, such as the one presented, typically require order N^q, with $1 \leqslant q \leqslant 2$. For details see Axelsson [3]. Also, such solvers are highly advantageous since solutions to previous time steps can be used as the first guess to accelerate the solution procedure. We note that time step size adaptivity is paramount, since the tissue's dynamics can dramatically change over the course of time, requiring radically different time step sizes for a preset level of accuracy. However, one must respect an upper bound dictated by the discretization error, i.e. $\Delta t \leqslant \Delta t^{\mathrm{lim}}$.

A recursive iterative scheme of Jacobi-type, where the updates are made only after one complete iteration, was presented only for algebraic simplicity. The Jacobi method is easier to address theoretically, while the Gauss–Seidel type method, which involves immediately using the most current values, when they become available, is usually used at the implementation level. As is well known, under relatively general conditions, if the Jacobi method converges, the Gauss–Seidel method converges at a faster rate, while if the Jacobi method diverges, the Gauss–Seidel method diverges at a faster rate. For example, see Axelsson [3].

[5] This collapses to a stencil of $\ddot{\boldsymbol{r}}^{L+1} = \frac{\boldsymbol{r}^{L+1} - 2\boldsymbol{r}^{L} + \boldsymbol{r}^{L-1}}{(\Delta t)^2}$, when the time step size is uniform.

[6] For the class of problems under consideration, due to the quadratic dependency on Δt, $p \approx 2$.

[7] Typically, K_{d} is chosen to be between five to ten iterations.

An implementation of the overall (Gauss–Siedel) process, whose goal to determine the dynamic equilibrium for all of the (coupled) nodes, and to deliver solutions where the iterative consistency error is controlled and the temporal discretization accuracy dictates the upper limits on the time step size ($\Delta t^{\lim}$), is as follows:

$$
\begin{array}{l}
(1)\,\text{GLOBAL FIXED} - \text{POINT ITERATION}: \ (\text{SET i} = 1 \text{ AND K} = 0): \\
(2)\,\text{IF i} > \text{N THEN GO TO (4)} \\
(3)\,\text{IF i} \leq \text{N THEN}: \\
\quad (a)\,\text{COMPUTE MASS POSITION}: \boldsymbol{r}_i^{L+1,K} \approx \dfrac{\Delta t^2}{m_i}\left(\boldsymbol{\Psi}_i^{tot}(\boldsymbol{r}^{L+1,K-1})\right) + \boldsymbol{r}_i^L + \Delta t \dot{\boldsymbol{r}}_i^L \\
\quad (b)\ \text{GO TO (2) AND NEXT MASS (i} = \text{i} + 1) \\
\quad (a)\,\text{SOLVE FOR CAUCHY STRESSES}: \sigma_I^K = F_I^K S_I^{K-1} \\
\quad (a)\,\text{COMPUTE DAMAGE/RUPTURE IN EACH FIBER}: S_I^K \\
(4)\,\text{ERROR MEASURE}: \\
\quad (a) \varpi_K \stackrel{\text{def}}{=} \dfrac{\sum_{i=1}^N ||\boldsymbol{r}_i^{L+1,K} - \boldsymbol{r}_i^{L+1,K-1}||}{\sum_{i=1}^N ||\boldsymbol{r}_i^{L+1,K} - \boldsymbol{r}_i^{L}||} \qquad (\text{normalized}) \\
\quad (b) Z_K \stackrel{\text{def}}{=} \dfrac{\varpi_K}{TOL_r} \\
\quad (c) \Phi_K \stackrel{\text{def}}{=} \left(\dfrac{(\frac{TOL}{\varpi_0})^{\frac{1}{p K_d}}}{(\frac{\varpi_K}{\varpi_0})^{\frac{1}{p K}}} \right) \\
(5)\,\underline{\text{IF TOLERANCE MET } (Z_K \leq 1) \text{ AND } K < K_d \text{ THEN}:} \\
\quad (a)\,\text{INCREMENT TIME}: t = t + \Delta t \text{ AND GO TO (1)} \\
\quad (b)\,\text{CONSTRUCT NEW TIME STEP}: \Delta t = \Phi_K \Delta t \\
\quad (c)\,\text{SELECT MINIMUM}: \Delta t = MIN(\Delta t^{lim}, \Delta t) \\
(6)\,\underline{\text{IF TOLERANCE NOT MET } (Z_K > 1) \text{ AND } K = K_d \text{ THEN}:} \\
\quad (a)\,\text{CONSTRUCT NEW TIME STEP}: \Delta t = \Phi_K \Delta t \\
\quad (b)\,\text{RESTART AT TIME} = \text{t AND GO TO (1)}
\end{array}
\tag{4.14}
$$

Remark 1. At the implementation level in Box (4.14), normalized (nondimensional) error measures were used. As with the unnormalized case, one approximates the error within an iteration to behave according to

$$
(\gamma(\Delta t)^p)^K \underbrace{\frac{\|\boldsymbol{r}^{L+1,1} - \boldsymbol{r}^{L+1,0}\|}{\|\boldsymbol{r}^{L+1,0} - \boldsymbol{r}^{L}\|}}_{\varpi_0} = \underbrace{\frac{\|\boldsymbol{r}^{L+1,K} - \boldsymbol{r}^{L+1,K-1}\|}{\|\boldsymbol{r}^{L+1,K} - \boldsymbol{r}^{L}\|}}_{\varpi_K}, \quad K = 2, \ldots \tag{4.15}
$$

where the normalized measures characterize the ratio of the iterative error within a time step to the difference in solutions between time steps. Since both $\|\boldsymbol{r}^{L+1,0} - \boldsymbol{r}^{L}\| = \mathcal{O}(\Delta t)$ and $\|\boldsymbol{r}^{L+1,K} - \boldsymbol{r}^{L}\| = \mathcal{O}(\Delta t)$ the approach has roughly the same rates of convergence, and the adaptive scheme remains the same. The normalized measures are preferred since they have a clear meaning.

Remark 2. The use of pinned-joints, i.e. not allowing moments at each node, greatly speeds up the computation in this approach. Bending can be taken into account, and adds a degree of complexity that may be warranted in certain applications. It is still rather unclear exactly how, for example, collagen fibers in a network are connected to one another and the degree to which those connections may or may not support moments. Probably, there are situations where the adopted simplification could be adequate, and others where it is not. Also, as mentioned previously, we ignore buckling phenomena and consider cases where compressive stresses are of somewhat less importance than tensile states. However, the objective of this paper is simply to illustrate the main modeling and solution techniques, without overly complicating issues. In other words, this model and solution technique serves as a starting point for more in-depth analyses.

5. Numerical simulation: pressurized loading

As an idealized model problem, we consider a planar rectangular sheet, composed of the fiber network, clamped on all four edges. We consider gradually increasing forces due to pressure loading underneath the tissue, for each node, of the form:

$$
\mathscr{F} = \frac{f_0 D^2 \mathrm{e}^{qt}}{N}, \tag{5.1}
$$

where f_0 is a pressure force constant, D is the length of a side of the square ($D \times D$) exterior membrane boundary, q is a loading rate parameter and where N is the total number of nodes. The unit normal at a node is computed by taking the cross-product of the vectors connecting the nodes before and after the node in question, and normalizing the result by the magnitude. The pressure is then projected onto this normal, $\boldsymbol{n}$. Thus, this is *live loading*, since each nodal $\boldsymbol{n}$ is a function of the deformation. In order to illustrate the robustness of the approach, the tissue was given some heterogeneity from fiber to fiber: a 50% variation from a mean overall value of the material constant c for the fibers (Fig. 1). Also, an initially softened elliptical region was placed slightly off center in the tissue

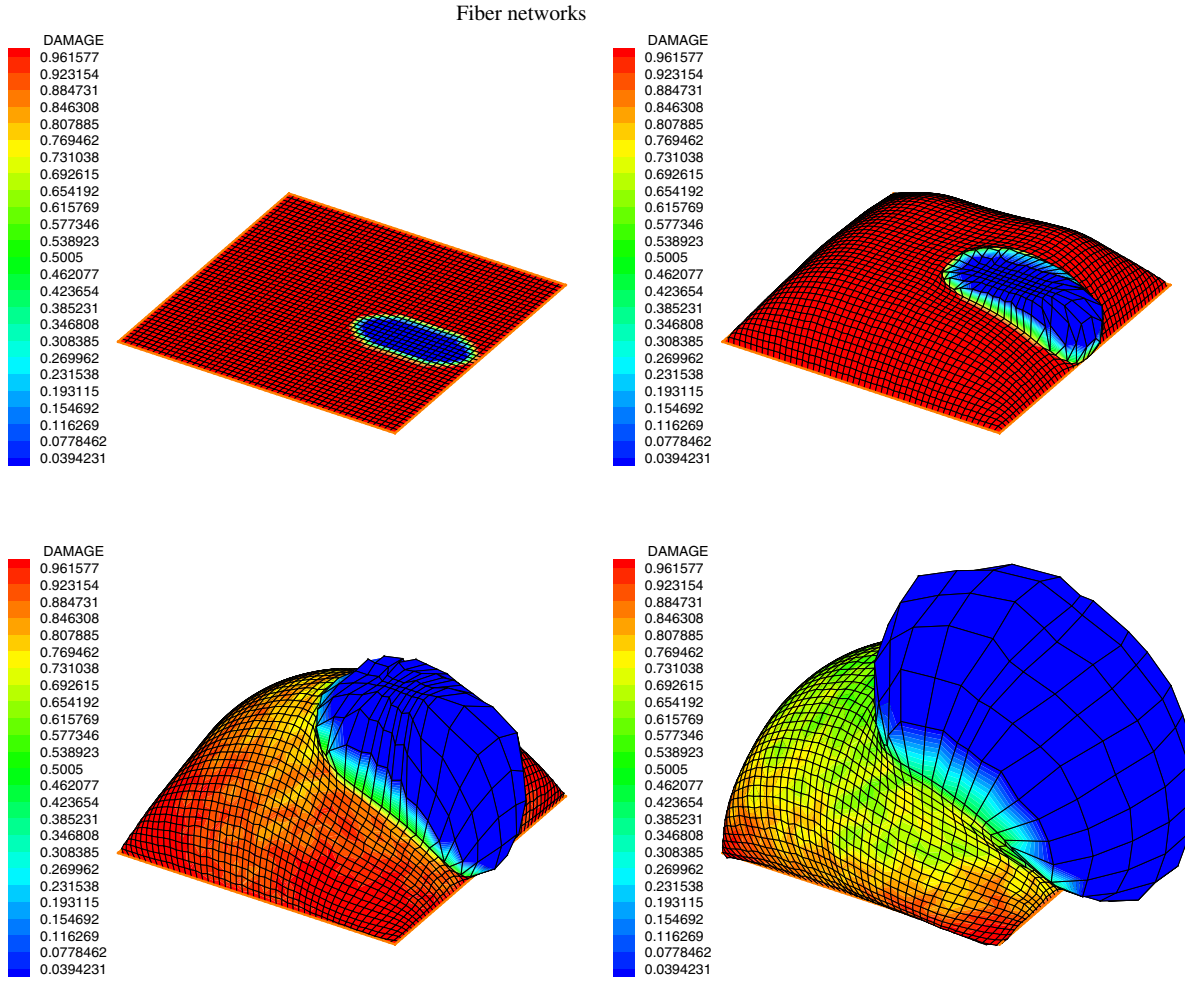

Fig. 2. Starting from the top, left to right: Successive frames of the pressurized loading leading to rupture. The graphics indicate the average damage in the surrounding fibers.

(Fig. 2). A 50×50 network was used. The specific parameters employed were:

- The initial radii of the fibers were $r_0 = 10^{-5}$ m.
- The dimensions of the domain were 0.025 m $\times$ 0.025 m.
- The starting time step value, $\Delta t = 0.005$ s.
- The iterative stopping tolerance, $\mathrm{TOL}_r = 0.001$.
- The total simulation time, $T = 10$ s.
- The desired number of iterations, $K_{\mathrm{d}} = 20$.
- The upper bound on the time step size, $\Delta t^{\mathrm{lim}} = 0.01$ s.
- The initial pressure, $f_0 = 0.00001$ Pa.
- The pressure rate, $q = 1.0$.
- The damage rate, $\lambda = 1$.
- The critical stretch, $U_{\mathrm{crit}} = 1.25$.
- The Fung material parameters were $c = (1 \pm 0.5) \times 10^5$ Pa and $H = 10^{-3}$.
- The first Fung material parameter in the weakened elliptical region was one-hundredth of the nominal; $c = (1 \pm 0.5) \times 10^4$ Pa (H was the same).
- The major radius of the elliptical softened region was 0.005 m, while the minor radius of the elliptical softened region was 0.0025 m.

As Fig. 3 indicates, it takes some time for the critical stretch to be met before damage starts to occur. Thus, in the beginning, the time step sizes are enlarged, automatically by the algorithm, until the (finite difference) discretization error upper limit (set to $\Delta t^{\mathrm{lim}} = 0.01$) was met. Thereafter, when damage initiates, inhomogeneously (Fig. 2), the steps are refined and unrefined to meet the iterative error tolerance. At this stage in the deformation, the iterative error tolerance dictates time step sizes which are required, by the adaptive algorithm, to be smaller than the step-size dictated by the discretization limit. Clearly, the method can handle extraordinarily large, inelastic, deformations that would be difficult to formulate with an anisotropic continuum theory, and an accompanying finite element discretization. The total simulation time was on the order of 45 s on a standard 2.33 GHz laptop.

Remark. The model presented is flexible enough to capture static or dynamic loading. We remark that although usually quasistatic loading with time-varying boundary conditions are appropriate for most biomechanical applications, there are cases, for example blunt trauma-type

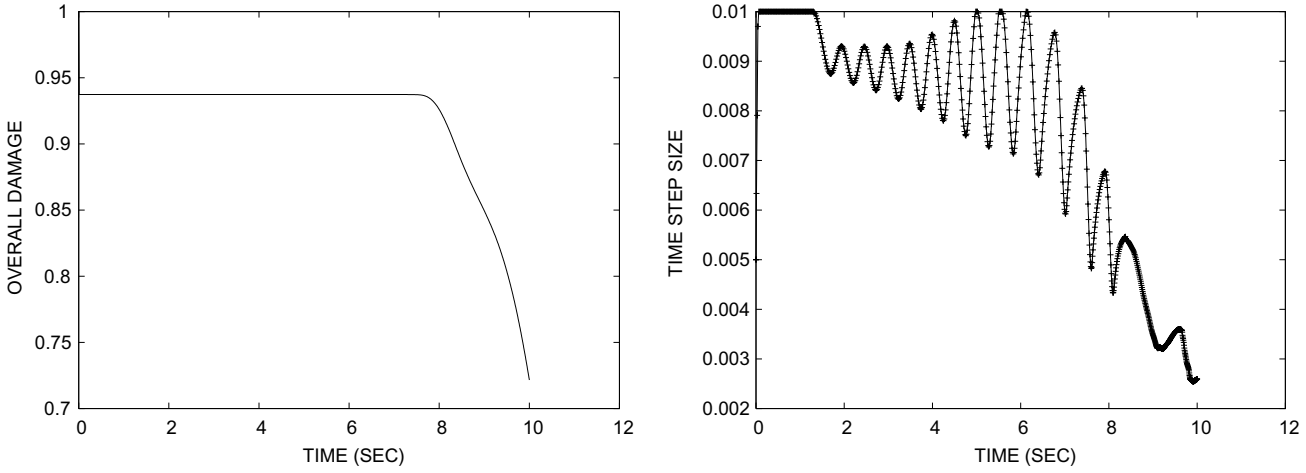

Fig. 3. Left: The overall damage, $\langle \alpha \rangle_{\Omega} \stackrel{\text{def}}{=} \frac{1}{|\Omega|} \int_{\Omega} \alpha \, d\Omega$, of the tissue. *Note:* there was approximately 7% initial damage due to the initially softened elliptical region in the tissue (Fig. 2). Right: The time step sizes versus time.

loading where dynamic loading is important. Clearly, if the inertial terms are made small, by allowing $m \rightarrow 0$, the response will resemble a quasistatic solution, if that is desired. As mentioned previously, this type of approach is sometimes referred to as a psuedo-dynamical solution technique to solve quasistatic problems [50,17–19,1,2,43].

6. Summary and future work

The purpose of this paper was to present an accessible, straightforward, modeling approach, which can be numerically implemented with minimal effort by researchers interested in the simulation of fibrous biological tissue. In summary, the advantages of such a fiber network approach are that the constitutive laws at the (one-dimensional) fiber level are simple and that the damage and rupture therein is straightforward to characterize. Additionally, the model is amenable to extremely rapid numerical simulation. The purpose of the presented work was simply to illustrate how the approach works, since it is quite flexible, and adaptable to specific applications. Clearly, for most applications, specific material data is needed for the fibrous tissue. In particular, the properties of soft tissue need to be specified and incorporated in future analyses. The major points for improvement are (1) incorporation of more realistic fiber arrangements (perhaps involving stochastic spatial perturbations) and inter-fiber connections, (2) incorporation of the soft tissue surrounding the fibers and (3) incorporation of clinical and experimental results.

Generally, because the distribution of water, biological fluids and chemical species within such tissue are dependent on the deformation of the solid, coupled multifield computations are necessary to realistically simulate such systems. For example, in many models involving fibrous biological tissue, it is usually assumed that the response depends on the concentration of a chemical species present, denoted s, for example, intracellular calcium Ca^{2+}, and the stretch U of the tissue fiber relative to a reference sarcomere length. A basic form suggested is $\sigma = \sigma(s, U)$, where σ is the total Cauchy stress (active and passive), which combines the mechanical (passive) contribution and the actively generated muscle tension. There exist several models for incorporating the effects of a chemical species into the response of biotissue. For example, consider $\sigma = \sigma^{\text{mech}} + \sigma^{\text{chem}}(Ca^{2+}, U)$, where σ is the total Cauchy stress (active and passive), σ^{mech} is the usual mechanical (passive) contribution, $\sigma(Ca^{2+}, U)$ is the actively generated muscle tension and where U is the stretch along the muscle fiber. See Rachev and Hayashi [45], Humphrey [25] or [26] for reviews.[8] A proto-typical coupled system involves (a) fluid mechanics, involving the concentration of suspensions, which are nominally convected with the fluid, (b) fluid–solid interaction at wall/fluid interfaces, leading to penetration or absorption of suspensions into the biotissue and (c) growth of the tissue and an accompanying buildup of stress and/or possible damage. Staggering schemes are clearly ideal to simulate such processes (see, for example, [48,53,38,37,11,12,54–58]). Also see, for example, Zohdi et al. [59] and Zohdi [60] for simple cases involving coupled fields associated with atherosclerosis. Generally, such schemes proceed, within a discretized time step, by solving each field equation individually, allowing only the corresponding primary field variable to be active. This effectively decouples the system of differential equations. After the solution of each field equation, the primary field variable is updated, and the next field equation is solved in a similar manner, with only the corresponding primary variable being active. For accurate numerical solutions, the approach requires small time steps, primarily because the staggering error accumulates with each passing increment. Generally, such computations will require time step

[8] The system presented in this paper can be considered a relatively simple coupled system, coupling equilibrium and damage equations.

adaptivity, perhaps, for example, using schemes such as the one presented in this work. We note that this staggering-type approach could be used for systems with two families of interacting fibers, representing two types of tissue, for example elastin and collagen.

Current work of the author is seeking to describe the rupture of fibrous cap tissue which forms during plaque growth associated with the vascular disease of atherosclerosis. Myocardial infarction and stroke can result from fibrous plaque cap rupture and subsequent release of highly thrombogenic material and lipids into the blood stream. Lesions (plaque caps) with a high risk of rupture are termed *vulnerable* (see, for example [16]), and are responsible, along with other micromorphological characteristics, such as lipid core size, for many sudden life-threatening cardiovascular events. For example see Shah [49], Virmani et al. [51], van der Wal and Becker [52], Chyu and Shah [8], Libby and Aikawa [39], Libby [40], Richardson et al. [46], Loree et al. [41] and Davies et al. [10] for overviews.

References

[1] A.A. Atai, D.J. Steigmann, On the nonlinear mechanics of discrete networks, Arch. Appl. Mech. 67 (1997) 303–319.

[2] A.A. Atai, D.J. Steigmann, Coupled deformations of elastic curves and surfaces, Int. J. Solids Struct. 35 (16) (1998) 1915–1952.

[3] O. Axelsson, Iterative Solution Methods, Cambridge University Press, 1994.

[4] H.A. Buchholdt, M. Davies, M.J.L. Hussey, The analysis of cable nets, J. Inst. Math. Appl. 4 (1968) 339–358.

[5] H. Bufler, B. Nguyen-Tuong, On the work theorems in nonlinear network theory, Ing. Arch. 49 (1980) 275–286.

[6] M. Cannarozzi, A minimum principle for tractions in the elastostatics of cable networks, Int. J. Solids Struct. 23 (1987) 551–568.

[7] M. Cannarozzi, Stationary and extremum variational formulations for the elastostatics of cable networks, Meccanica 20 (1985) 136–143.

[8] K.Y. Chyu, P.K. Shah, The role of inflammation in plaque disruption and thrombosis, Rev. Cardiovas. Med. 2 (2001) 82–91.

[9] K.D. Costa, J.W. Holmes, A.D. McCulloch, Modeling cardiac mechanical properties in three dimensions, Philos. Trans. R. Soc. Lond. A 359 (2001) 1233–1250.

[10] M.J. Davies, P.D. Richardson, N. Woolf, D.R. Katz, J. Mann, Risk of thrombosis in human atherosclerotic plaques: role of extracellular lipid, macrophage, and smooth muscle cell content, Br. Heart J. 69 (1993) 377–381.

[11] St. I. Doltsinis, Coupled field problems–solution techniques for sequential and parallel processing, in: M. Papadrakakis (Ed.), Solving Large-scale Problems in Mechanics, 1993.

[12] I.St. Doltsinis, Solution of coupled systems by distinct operators, Engrg. Comput. 14 (1997) 829–868.

[13] Y.C. Fung, On the foundations of biomechanics, ASME J. Appl. Mech. 50 (1983) 1003–1009.

[14] Y.C. Fung, Biorheology of soft tissues, Biorheology 10 (1973) 139–155.

[15] Y.C. Fung, Elasticity of soft tissues in simple elongation, Am. J. Physiol. 28 (1967) 1532–1544.

[16] V. Fuster, Assessing and Modifying the Vulnerable Atherosclerotic Plaque, Futura Publishing Company, 2002.

[17] E.M. Haseganu, D.J. Steigmann, Analysis of partly wrinkled membranes by the method of dynamic relaxation, Comput. Mech. 14 (1994) 596–614.

[18] E.M. Haseganu, D.J. Steigmann, Theoretical flexural response of a pressurized cylindrical membrane, Int. J. Solids Struct. 31 (1994) 27–50.

[19] E.M. Haseganu, D.J. Steigmann, Equilibrium analysis of finitely deformed elastic networks, Comput. Mech. 17 (1996) 359–373.

[20] G.A. Holzapfel, M. Stadler, C.A.J. Schultze-Bauer, A layer-specific three-dimensional model for the simulation of balloon angioplasty using magnetic resonance imaging and mechanical testing, Ann. Biomed. Engrg. 30 (2002) 753–767.

[21] G.A. Holzapfel, Biomechanics of soft tissue, in: J. Lemaitre (Ed.), The Handbook of Materials Behavior Models, Multiphysics Behaviors, Composite Media, Biomaterials, vol. III, Academic Press, Boston, 2001, pp. 1049–1063 (Chapter 10).

[22] G.A. Holzapfel, T.C. Gasser, A viscoelastic model for fiber-reinforced composites at finite strains: continuum basis, computational aspects and applications, Comput. Methods Appl. Mech. Engrg. 190 (2001) 4379–4403.

[23] G.A. Holzapfel, T.C. Gasser, R.W. Ogden, A new framework for arterial wall mechanics and a comparative study of material models, J. Elasticity 61 (2000) 1–48.

[24] G.A. Holzapfel, H.W. Weizsäcker, Biomechanical behavior of the arterial wall and its numerical characterization, Comput. Biol. Med. 28 (1998) 377–392.

[25] J.D. Humphrey, Continuum biomechanics of soft biological tissues, Proc. R. Soc. 459 (2029) (2003) 3–46.

[26] J.D. Humphrey, Cardiovascular Solid Mechanics, Cells, Tissues and Organs, Springer-Verlag, New York, 2002.

[27] J.D. Humphrey, R.L. Barazotto, W.C. Hunter, Finite extension and torsion of papillary muscles: theoretical framework, J. Biomech. 25 (1992) 541–547.

[28] J.D. Humphrey, R.K. Strumpf, F.C.P. Yin, A constitutive theory for biomembranes: application to epicardium, ASME J. Biomech. Engrg. 114 (1992) 461–466.

[29] J.D. Humphrey, H.R. Halperin, F.C.P. Yin, Small indentation superimposed on a finite biaxial stretch: implications for cardiac mechanics, ASME J. Appl. Mech. 58 (1991) 1108–1111.

[30] J.D. Humphrey, R.K. Strumpf, F.C.P. Yin, Determination of a constitutive relation for passive myocardium: I. new functional form, ASME J. Biomech. Engrg. 112 (1990) 333–340.

[31] J.D. Humphrey, R.K. Strumpf, F.C.P. Yin, Determination of a constitutive relation for passive myocardium: II. Parameter estimation, ASME J. Biomech. Engrg. 112 (1990) 340–346.

[32] J.D. Humphrey, R.K. Strumpf, F.C.P. Yin, Biaxial mechanical behavior of excised ventricular epicardium, Am. J. Physiol. 259 (1990) H101–H108.

[33] J.D. Humphrey, F.C.P. Yin, Biomechanical experiments on excised myocardium: theoretical considerations, J. Biomech. 22 (1989) 377–383.

[34] J.D. Humphrey, F.C.P. Yin, Constitutive relations and finite deformations of passive cardiac tissue. II. Stress analysis in the left ventricle, Circ. Res. 65 (1988) 805–817.

[35] J.D. Humphrey, F.C.P. Yin, On constitutive relations and finite deformations of passive cardian tissue. I. A pseudostrain-energy function, ASME J. Biomech. Engrg. 109 (1987) 298–304.

[36] Y. Lanir, Constitutive equations for fibrous connective tissues, J. Biomech. 16 (1) (1983) 1–12.

[37] R.W. Lewis, B.A. Schrefler, The Finite Element Method in the Static and Dynamic Deformation and Consolidation of Porous Media, second ed., Wiley Press, 1998.

[38] R.W. Lewis, B.A. Schrefler, L. Simoni, Coupling versus uncoupling in soil consolidation, Int. J. Numer. Anal. Methods Geomech. 15 (1992) 533–548.

[39] P. Libby, The vascular biology of atherosclerosis, in: E. Braunwald, D.P. Zipes, P. Libby (Eds.), Heart Disease. A Textbook of Cardiovascular Medicine, sixth., W. B. Saunders Company, Philadelphia, 2001, pp. 995–1009 (Chapter 30).

[40] P. Libby, P.M. Ridker, A. Maseri, Inflammation and atherosclerosis, Circulation 105 (2002) 1135–1143.

[41] H.M. Loree, R.D. Kamm, R.G. Stringfellow, R.T. Lee, Effects of fibrous cap thickness on peak circumferential stress in model atherosclerotic vessels, Circ. Res. 71 (1992) 850–858.

[42] P.D. Pangiotopoulos, A variational inequality approach to the inelastic stress-unilateral analysis of cable structures, Comput. Struct. 6 (1976) 133–139.
[43] M. Papadrakakis, A method for the automatic evaluation of the dynamic relaxation parameters, Comput. Methods Appl. Mech. Engrg. 25 (1980) 35–48.
[44] A.C. Pipkin, The relaxed energy density for isotropic elastic membranes, IMA J. Appl. Math. 36 (1986) 297–308.
[45] A. Rachev, K. Hayashi, Theoretical study of the effects of vascular smooth muscle contraction on strain and stress distributions in arteries, Ann. Biomed. Engrg. 27 (1999) 459–468.
[46] P.D. Richardson, M.J. Davies, G.V.R. Born, Influence of plaque configuration and stress distribution on fissuring of coronary atherosclerotic plaques, Lancet 2 (8669) (1989) 941–944.
[47] M.S. Sacks, W. Sun, Multiaxial mechanical behavior of biological materials, Ann. Rev. Biomed. Engrg. 5 (2003) 251–284.
[48] B.A. Schrefler, A partitioned solution procedure for geothermal reservoir analysis, Commun. Appl. Numer. Methods 1 (1985) 53–56.
[49] P.K. Shah, Plaque disruption and coronary thrombosis: new insight into pathogenesis and prevention, Clin. Cardiol. 20 (Suppl. II) (1997) II-38–II-44.
[50] D.J. Steigmann, Tension field theory, Proc. R. Soc. London A 429 (1990) 141–173.
[51] R. Virmani, F.D. Kolodgie, A.P. Burke, A. Farb, S.M. Schwartz, Lessons from sudden coronary death: a comprehensive morphological classification scheme for atherosclerotic lesions, Arterioscl. Thromb. Vasc. Biol. 20 (2000) 1262–1275.
[52] A.C. van der Wal, A.E. Becker, Atherosclerotic plaque rupture – pathologic basis of plaque stability and instability, Cardiovasc. Res. 41 (1999) 334–344.
[53] O.C. Zienkiewicz, Coupled problems and their numerical solution, in: R.W. Lewis, P. Bettes, E. Hinton (Eds.), Numerical Methods in Coupled Systems, Wiley, Chichester, 1984, pp. 35–58.
[54] T.I. Zohdi, An adaptive–recursive staggering strategy for simulating multifield coupled processes in microheterogeneous solids, Int. J. Numer. Methods Engrg. 53 (2002) 1511–1532.
[55] T.I. Zohdi, Computational design of swarms, Int. J. Numer. Methods Engrg. 57 (2003) 2205–2219.
[56] T.I. Zohdi, Modeling and simulation of a class of coupled thermo-chemo-mechanical processes in multiphase solids, Comput. Methods Appl. Mech. Engrg. 193 (6–8) (2004) 679–699.
[57] T.I. Zohdi, Modeling and direct simulation of near-field granular flows, Int. J. Solids Struct. 42 (2) (2004) 539–564.
[58] T.I. Zohdi, Charge-induced clustering in multifield granular flow, Int. J. Numer. Methods Engrg. 62 (7) (2005) 870–898.
[59] T.I. Zohdi, G.A. Holzapfel, S.A. Berger, A phenomenological model for atherosclerotic plaque growth and rupture, J. Theor. Biol. 227 (3) (2004) 437–443.
[60] T.I. Zohdi, A simple model for shear stress mediated lumen reduction in blood vessels, Biomech. Model. Mechanobiol. 4 (1) (2005) 57–61.
[61] T.I. Zohdi, D.J. Steigmann, The toughening effect of microscopic filament misalignment on macroscopic fabric response, Int. J. Fract. 115 (2002) L9–L14.
[62] T.I. Zohdi, Modeling and simulation of progressive penetration of multilayered ballistic fabric shielding, Comput. Mech. 29 (2002) 61–67.
[63] T.I. Zohdi, D. Powell, Multiscale construction and large-scale simulation of structural fabric undergoing ballistic impact, Comput. Methods Appl. Mech. Engrg. 195 (1–3) (2006) 94–109.